Countermeasure of Multispectral Camouflage Nets to Imaging Spectroscopy

Santiago A. Rodriguez[1, 3], Michal Shimoni[2], Javier Plaza[1], Antonio Plaza[1], Ingmar Renhorn[4], Jörgen Ahlberg[4,5], Marijke Vandewal[2]

[1.] Hyperspectral Computing Laboratory, University of Extremadura, Cáceres, SPAIN.
[2.] Signal and Image Centre, Belgian Royal Military Academy, Brussels, BELGIUM.
[3.] National University of Cordoba (UNC), Cordoba, ARGENTINA.
[4.] Glana Sensors AB, Linköping, SWEDEN.
[5.] Computer Vision Laboratory, Linköping University, Linköping, SWEDEN.

santiagoarodriguez@gmail.com

ABSTRACT

In the last decade, the NATO nations progressed from conventional netting of camouflage to multispectral/polyspectral technology. This development, which is known also under the names stealth and 3rd generation technology, is a countermeasure to detection by radar, optical visible and infrared and acoustic sensors.

This work presents the assessment of 3rd generation woodland nets as a countermeasure to hyperspectral imaging. The analysis is done at three different levels of difficulty; (1) using calibration spectra and simulated images; (2) at operational background; and (3) by concealing objects in an operational environment. The scenes were scanned using L4 hyperspectral imager from Glana Sensors. This sensor consists of state-of-the-art variable optical filters running in 2D spatial mode. By making use of this innovative approach, the imager provides 48 independent spectral bands and high spatial resolution in the VNIR range of 450-950 nm.

Several detection methods were applied to scenes under various illuminations and operational difficulties. The results are reported and compared to the detection of 2D and 2nd generation camouflage nets available within the Belgian Defence.

1.0 INTRODUCTION

Multispectral camouflage is a counter-surveillance technique to conceal object from detection along several waverange of the electromagnetic spectrum. Traditionally, military camouflage has been designed to conceal an object in the visible spectrum. Multi-spectral camouflage advances this capability by contra measure to detection methods in the infrared and radar domains [1].

In the Near-Infra-Red (NIR), camouflage material is optimized for specific environment by tries to imitate the spectrum of vegetation, soil and man-made materials. Most advanced technology has satisfactory success in the VIS-NIR wavelengths (0.5-1.4 µm). However, beyond this wavelength range, the attempt to imitate the signature from biomass or clay minerals is accomplished with limited success. One of the reasons that military detectors are operated in the Short-Wave-Infrared (SWIR; 1.8-2.5 µm) part of the electromagnetic spectrum is associated to discrimination of camouflage materials [2], [15].

In the past few years, several sensors have been tested in the paradigm of detecting hidden objects [3]-[4]. Hyperspectral imaging (HSI) showed enormous success in defeating camouflage and occluded targets. Its large spectral range and high spectral resolution is employed in discriminating between camouflaged targets and backgrounds and revealing the occluded object [5], [14].

This paper presents the results of a study that assess the capability of hyperspectral imaging to conceal camouflaged woodland nets using miniature on-shelf HSI. The tests involve the measurement of 2nd and 3rd generations and 2D and 3D woodland nets using HSI in different scenarios and under various environmental conditions. Specifically, the following scenarios are discussed:

- Scenario 1 - Simulated images using laboratory spectral measurements;

- Scenario 2 - Measurements of camouflage nets in operational woodland scene;

- Scenario 3 - Measurements of concealed vehicle in operational woodland scene.

The results of several detection methods without and with priority knowledge are discussed as well as the comparison to 2nd generation net available within the Belgian Defence.

2.0   CAMOUFLAGE NETS UNDER EVALUATION

During the calibration phase and field tests, eight woodland camouflage nets were tested from different suppliers. The nets that are presented in Figure 2-1 are made from different fabrics and they are classified based on their texture and compositions. In 2D camouflage net, the concealed materials are integrated and printed into the net itself (Nets 3, 5 and 7 in Figure 2-1). 3D net is composed from blending structures that can move with wind (Nets 1, 2, 4, 6) or made from reversible tarp (Net 8). Net-6 is a 2nd generation and 3D net is available within the Belgian Defence. This woodland net conceals an object against optical VIS-NIR spectral measures. All the other nets are classified as 3rd generation. These are composed of 2 to 3 layers of nets or reversible net that conceal an object against multi-spectral detectors (i.e. VIS-NIR, infrared and microwave). Table 2-1 summarizes the category of each net under evaluation.

Figure 2-1: Camouflage nets under evaluation.

Table 2-1: Camouflage nets categories

Net ID	Category
1	3rd Generation. 3D
2	3rd Generation. 3D
3	3rd Generation. 2D
4	3rd Generation. 3D
5	3rd Generation. 2D
6	2nd Generation. 3D
7	3rd Generation. 2D
8	3rd Generation. 3D

3.0 METHODOLOGY

3.1 The hyperspectral sensor

The miniature hyperspectral imager, L4 developed by Glana Sensors AB, was used in this study for spectral measurements. This advanced sensor is based on exponentially variable filter (EVF) which is attached on, or in the direct proximity to the detector plane (Figure 3-1). In the used prototype, the Bayer filter is replaced by the EVF in a digital machine vision camera. The bandpass EVF filter allows the light to pass only in a narrow wavelength band, centered at a wavelength λ_c. This center wavelength varies over the filter as a function of the pixel position (x, y). The center wavelength is a function of only one dimension according to $\lambda_c = \lambda_c(x)$. As the EVF is mounted on, or very close to the detector plane, the light registered by the sensor element at position (x, y) will only contain wavelengths close to $\lambda_c(x,y)$. When the camera and the observed surface are static, each point on the object will thus be observed in a specific wavelength [5]. By rotating the camera, it can be used as imager spectrometer, as described in [7].
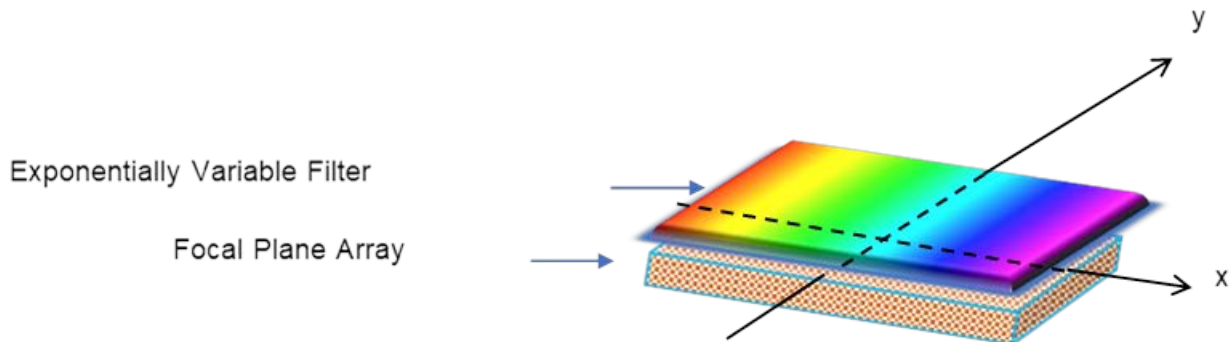
Figure 3-1: Exponentially Variable Filter.

3.2 Testing Setup

Reference spectra of the eight camouflage nets were collected indoor and outdoor for simulation and calibration, respectively. Indoor, the nets were measured using the ASD FieldSpec Pro FR in the spectral range of 350 nm to 2500 nm with a spectral resolution of 3 nm in the VNIR and 10 nm in the SWIR.
For calibration purposes and for collection of reference spectra, the L4 was used to measure the camouflage nets at mid-summer time, under clear sky condition and over known reflectance panels. Specifically, 5% calibration panel (Zenith SG3165) was placed behind the net and 20% (Zenith SG3164) calibration panel was positioned next to the net as presented in Figure 3-1.

Figure 3-1: Outdoors nets measurements with calibrated reflectance panels.

All the outdoors tests using the Glana-L4 were performed when the camera is mounted on tripod and scanned the field of view in horizontal direction. At scene meteorological parameters as ambient temperature, wind speed, atmospheric pressure, humidity and sun irradiation were monitored using dedicated station.

4.0 RESULTS

Prior to the operational measurements, a sensitivity analysis of the spectrometer was performed using the calibrated images. At first, the laboratory spectra of the camouflage nets were matched to the spectral resolution of GLANA-L4. The results are presented in Figure 4-1, right, show good features matching between the spectra collected by the ASD and GLANA-L4. Further, four spectral matching methods including the spectral angle mapper (SAM), spectral information divergence (SID), normalized spectral similarity score (NormXcorr) and root mean square error (RMSE) were used to validate the matching of the laboratory spectra to the spectra of the calibrated images. Descriptions of these methods can be found in [11]. The matching results of Net-1 using the spectra of the 'brown pattern' (i.e. soil) are presented in Figure 4-2.
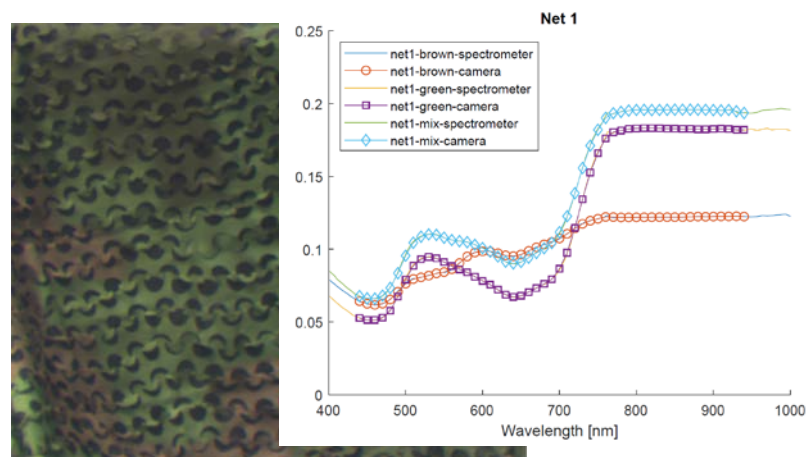
Figure 4-1: RGB representation of Net-1 [3rd generation and 3D] (left); Spectral matching of GLANA-L4 to the laboratory spectra collected using the ASD (right).

The results show good matching between the spectra of Net-1 (Figure 4-1 right) and the laboratory spectra (Figure 4-2). As expected, the SAM and the RMSE are resolved with very low scores in the soil pattern/color, whereas the SID and the NormXcorr with high scores. The matching of all the calibrated images, using the laboratory spectra, obtained similar successful matching. This ensured the use of the laboratory spectra for creating the simulated images discussed in section 4.1.
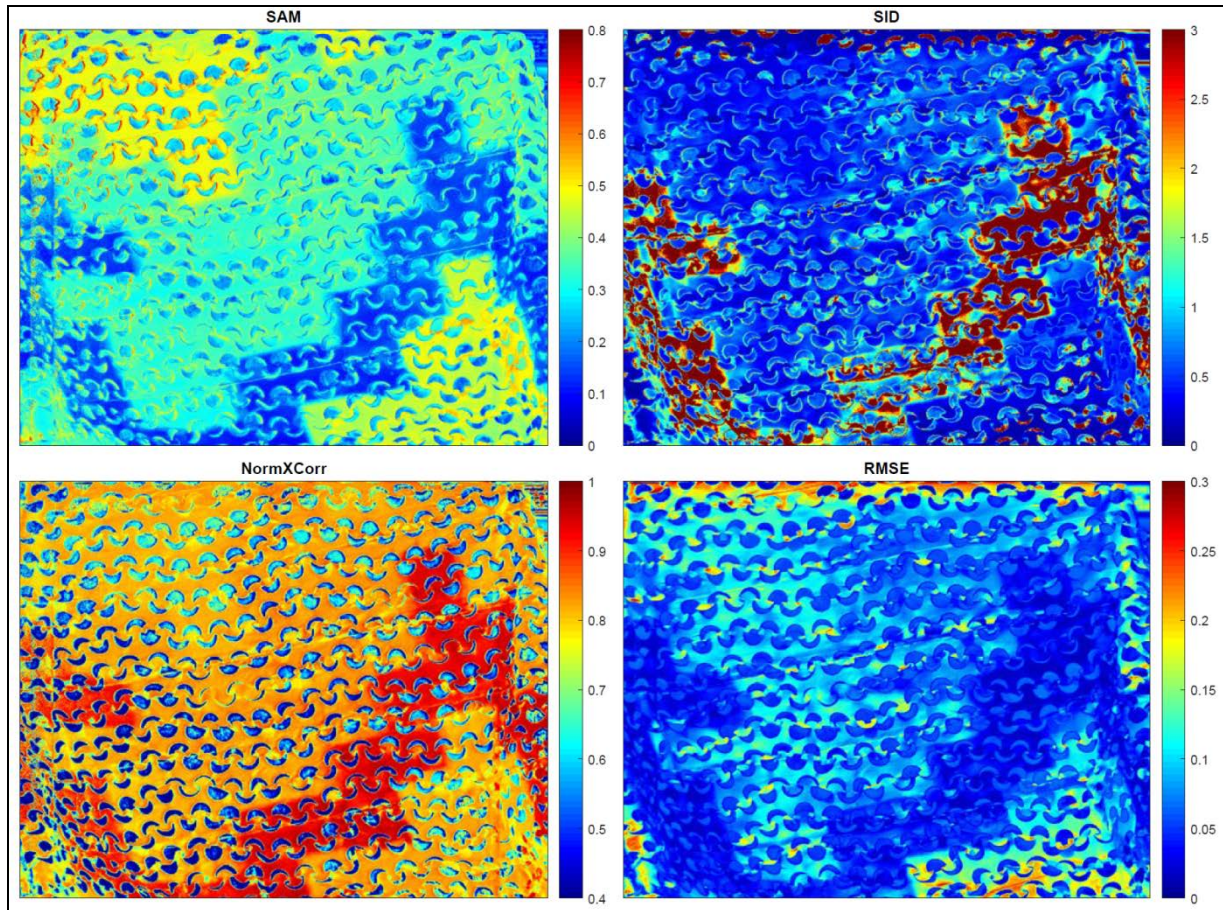
Figure 4-2: Spectral matching results of Net-1 [3rd generation and 3D].

4.1   Scenario 1 - Simulated images using indoor spectral measurements

Several synthetic images using different SNR and various mixing ratios of targets and background were created. The latter was generated using random composition of woodland spectra collected by USGS [12]. Further, an adaptive cosine estimator (ACE) [8] was used to detect the camouflage nets in the synthetic images. Figure 4-3 presents the target detection results for Net-6. The upper row shows that with low mixing rate of 90% target and 10% background it is possible to detect Net-6 at low and medium levels of noise (i.e. SNR=30 and 20 dB, respectively). However, at higher mixing rate of 50% target and 50% background (second row), only at low level of noise (i.e. SNR=30 dB) it is possible to separate the nets from the other nets. At this mixing rate with SNR=10 dB, the level of false alarms is higher than accepted for operational systems.
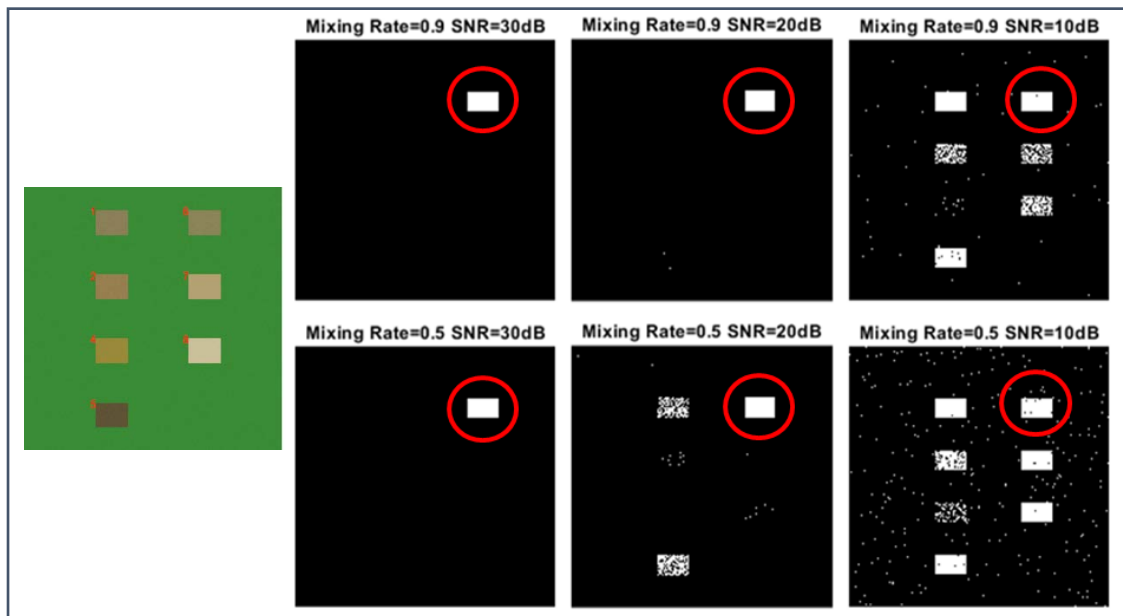
Figure 4-3: Detection of Net 6 using the ACE algorithm. Synthetic image of seven nets in woodland background (left); Detection results of targets are composed of 90% spectra of targets and 10% background with SNR of 30, 20 and 10 dB (upper row); Detection results of targets are composed of 50% spectra of targets and 50% background with SNR of 30, 20 and 10 dB (second row).

4.2 Scenario 2 - Measurements of camouflage nets in operational woodland scene

In Scenario-2, six missile cameras installed on tripods were covered with six different camouflage nets. The nets were positioned in front of North-European woodland (Figure 4-4) and scanned from a distance of about 200 meters (Figure 4-5).

Figure 4-4: GLANA-L4 image of Scenario-2. Nets 2 to 7 are positioned in front of a woodland background.

Figure 4-5: Setting of Scenario-2. The sensor is placed 200 meters from targets.

4.2.1 Detection without prior knowledge

The Local Anomaly Descriptor (LAD) [9] and the Orthogonal Subspace Projection-RX (OSP-RX) [10] detectors were applied to the hyperspectral image of Scenario-2 (Figure 4-6). The results show that the LAD could not separate the nets from the background and the implementation of OSP-RX resulted in very high level of false alarms. The reason for these unsatisfying results is originated from a spatial displacement between the spectral bands. For this scenario, the Glana-L4 was configured with a frame-rate 2 seconds for each independent band. This temporal delay produced spatial displacement of moving objects (leaves with the wind) between the bands. When this displacement occurs, a single pixel may obtain reflectance values that are correspondent to different materials.
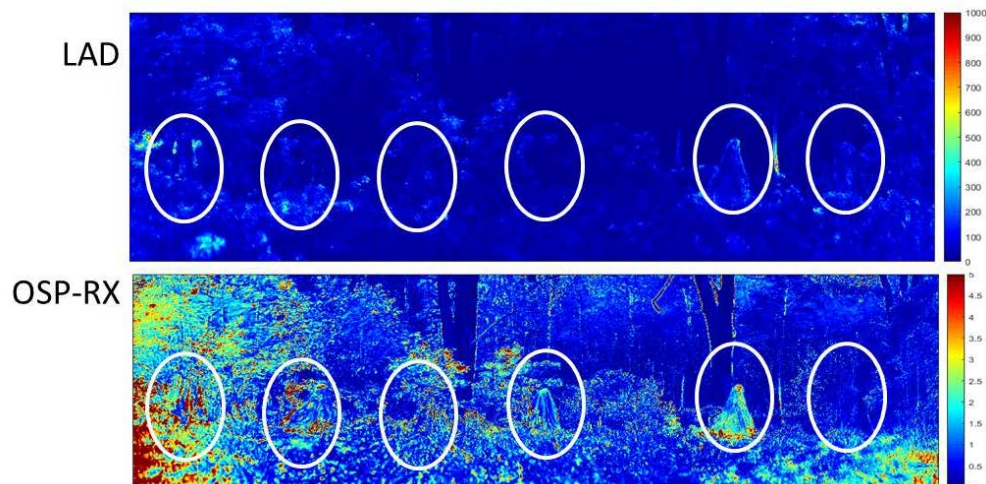
Figure 4-6: Scenario-2 - Anomaly detection results.

This artifact cannot be corrected in post-processing. However, a spectral gradient analysis can be used to mask out the pixels that corresponds to moving objects. In this analysis, a new hyperspectral cube is

generated using the 1st derivative of the spectrum in each pixel as described in Figure 4-7. The numeric derivative Z' is calculated for each pixel according to the following equation:

$$Z' = [z(2) - z(1); z(3) - z(2); ...; z(m) - z(m-1)]$$ [1]

where m is the number of bands.

Hyperspectral Cube

Z: Spectral
Coordinate

Y: Spatial Height
Coordinate

X: Spatial Width
Coordinate

Spectral Gradient Cube

Z': Spectral
Gradient
Coordinate

Y: Spatial Height
Coordinate

X: Spatial Width
Coordinate
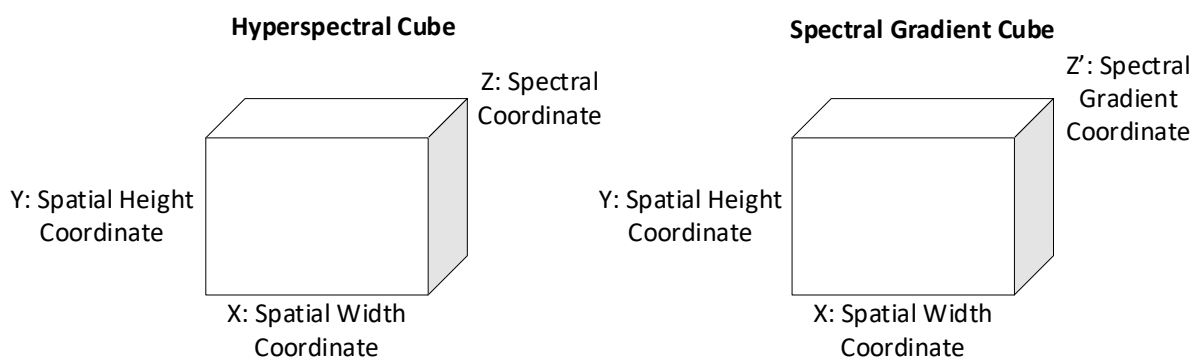
Figure 4-7: Spectral Gradient Cube generation for gradient analysis.

In similar way, all the spectra of vegetation are available in the catalogue of USGS [12] were also transformed using the 1st derivative and a referenced threshold using their reflectance was created. Following, the spectrum of each pixel in the hyperspectral image was evaluated in comparison to this reference as demonstrated in Figure 4-8. If a derivative spectrum is at the threshold values (i.e. left figure), the pixel is retained. If a derivative spectrum is outside the threshold (i.e. right image), the pixel is masked and not used further in the processing.
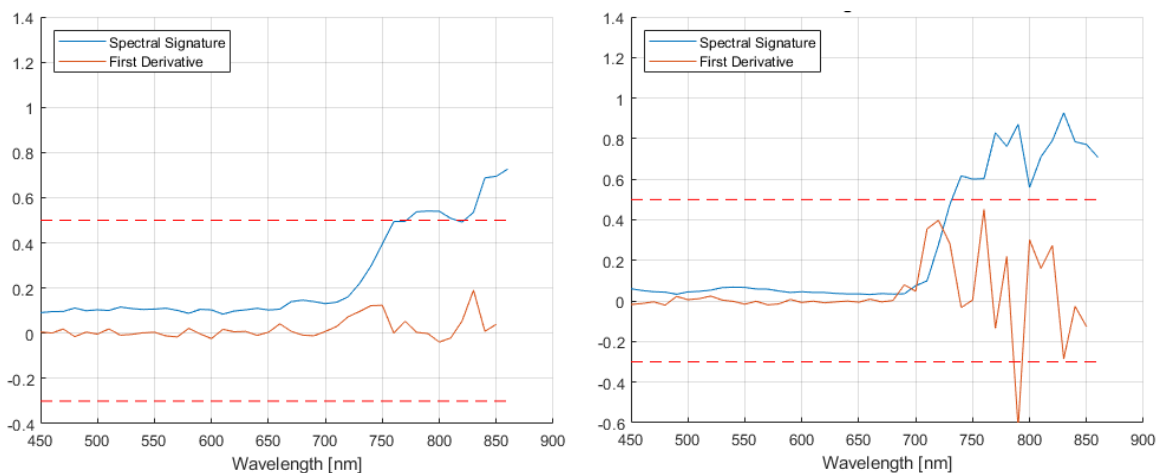
Figure 4-8: Masking using spectral gradient analysis. The original spectrum of a pixel (blue) and its derivative (orange).

The ROC curves of the anomaly detection, OSP-RX, before and after filtering are presented in Figure 4-9. An improvement of about 18% in detection is obtained after gradient filtering for the hyperspectral image is presented in Figure 4-4.
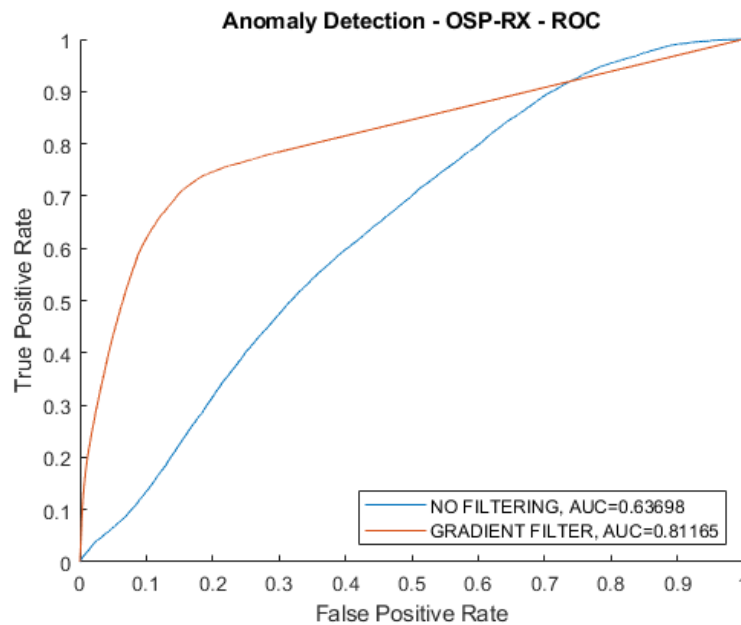
Figure 4-9: ROC curves for OSP-RX before and after gradient filtering.

4.2.2 Detection with prior knowledge

Following the achievement described in the previous section, four target detection methods using known spectra, were applied after implementing a gradient filter. The constrained energy minimization (CEM), the adaptive cosine estimator (ACE), the adaptive matched subspace detector (AMSD), and the orthogonal subspace projection (OSP) [13] were applied using the spectra of Nets 2, 5 and 6 and random background pixels collected from the scene.

The results of the detections of 3rd generation Nets 2 and 5, and their correspondent ROCs are presented in Figure 4-10. The results show difficulties to detect the 3rd generation and 3D net (Net 2) in comparison to the detection of 2D (Net 5). The number of false alarms is very high in the detection of Net-2 but the confusion is not with specific net, material or generation. In the case of Net-5, the number of false alarms is lower and the main confusion is with Net-6 (i.e. 2nd generation and 3D). The results of Net 2 and 5, also show large variation in the performances of the detection methods. CEM and OSP better detected Net-2 in comparison to ACE and AMSD. Opposite performances are observed for Net-5.

Figure 4-11 presents the detection results of Net-6 (2nd generation and 3D). The results show that all the applied methods detected Net-6 with different level of success. The best detection results with lower false alarms were achieved using CEM. By applying ACE and AMSD, the main confusion was obtained with Net-5. These results support the observation was discussed for Net-5 in the previous paragraph.
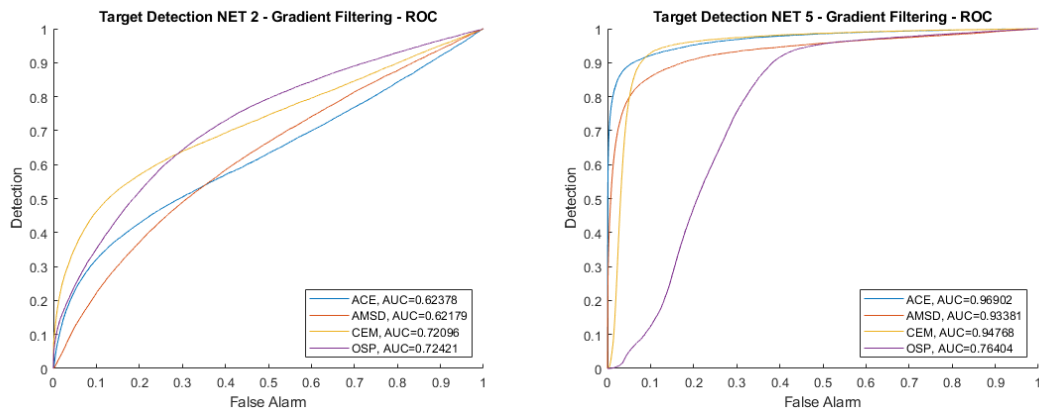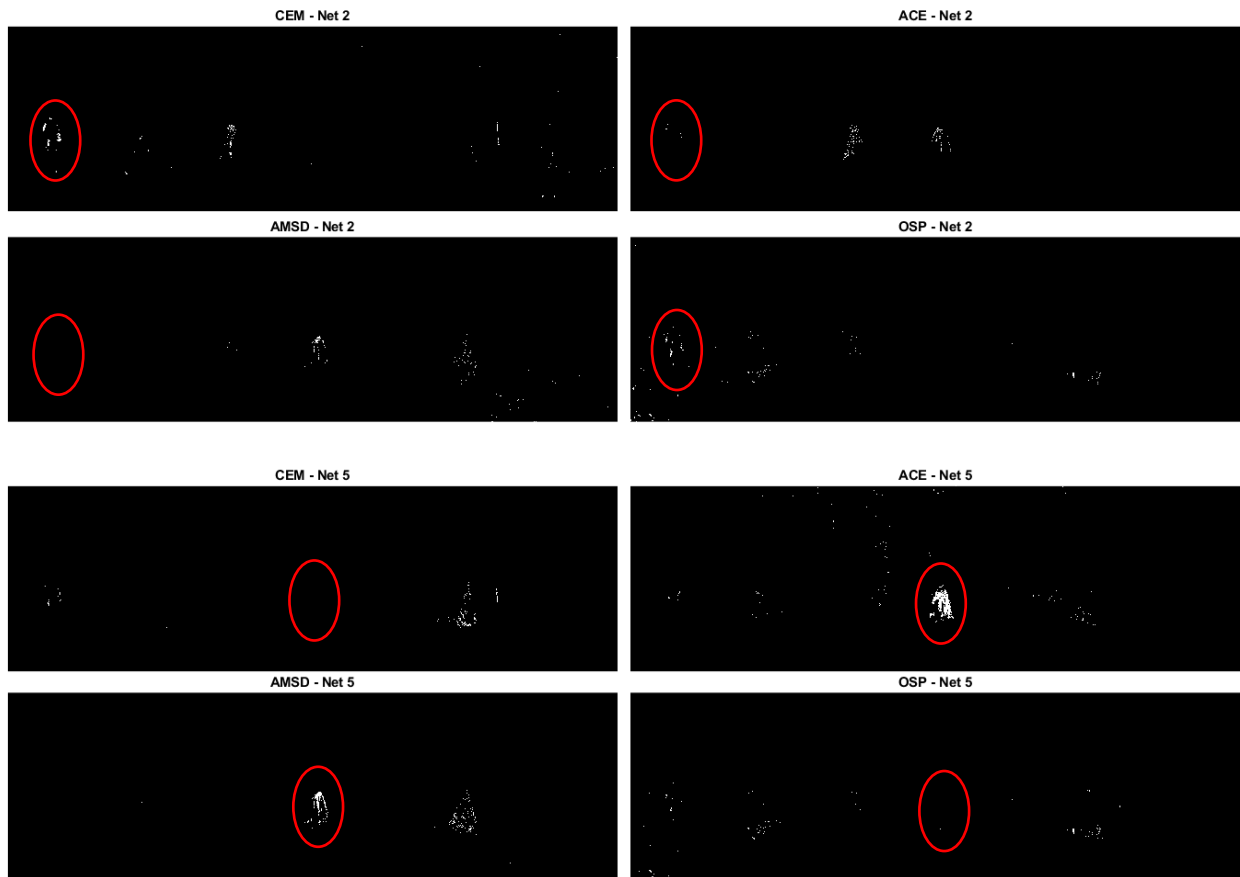
Figure 4-10: Detection with known spectra of Net 2 and 5.
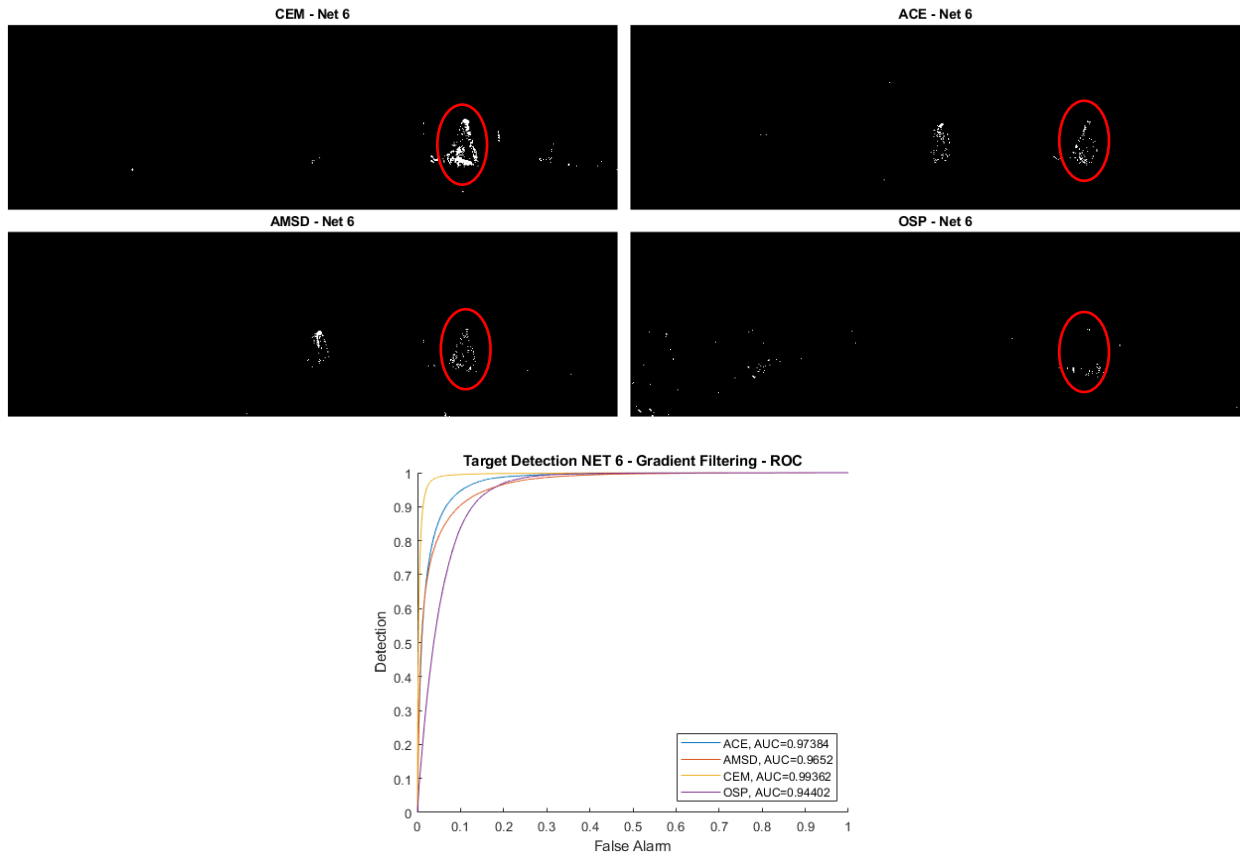
Figure 4-11: Detection with known spectra of Net-6.

4.3 Scenario 3 - Measurements of concealed vehicle in operational woodland scene

Scenario-3 presents realistic scene of near-detection by UAV (Figure 4-12). The object is scanned from near distance (~10 meters) and the number of background pixels is lower than the number of target pixels. In the scene, presented in Figure 4-12, Net 2 and 6 concealed a tank in the wood.
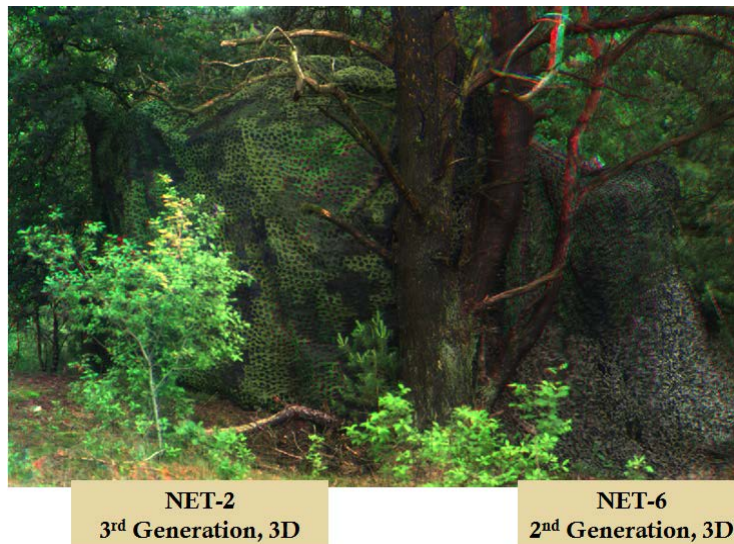
Figure 4-12: Hyperspectral image of concealed vehicle in operational woodland scene

As for the previous hyperspectral scene, a gradient filter was applied prior the implementation of the four detectors. The detection results for Net-2 and 6 are presented in Figure 4-13 and 4-14, respectively. The results show that the four methods detected Net-2 with different level of success but had difficulties to detect Net-6. In general, the performances of the detectors that required prior knowledge of the background spectra (i.e. AMSD and OSP) are inferior to the ones that require only the target spectra. The reason is that with low number of background pixels it is difficult to create a statistical model of the heterogeneous background and to separate the target vector from the background.
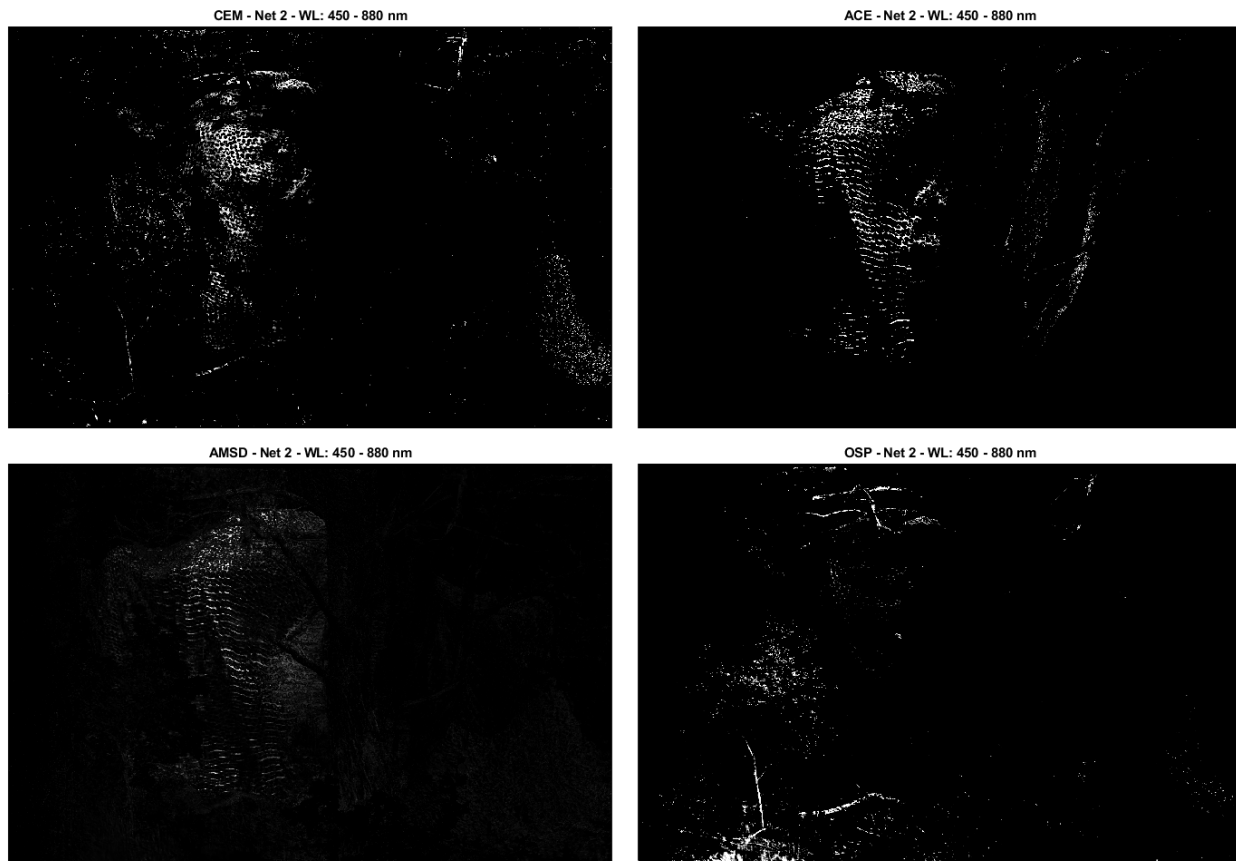
Figure 4-13: Scenario-3 - detection with known spectra of Net-2.

5.0   CONCLUSIONS

This study assesses the capability of miniature on-shelf hyperspectral imager to conceal camouflaged woodland nets in simulated and operational scenarios. The following findings can be summarized from the obtained results;

At operational woodland scene, without or with prior knowledge, it is difficult to detect 3rd generation camouflaged nets using the Glana L-4 sensor. It is possible to detect 2nd generation and 3D and 3rd generation and 2D nets in this scene, only after reducing the artifact effect due to large recording time. The detection of 2nd generation and 3D net is easily detected only if the number of background pixels is higher than the number of target pixels. The superiority of the 3rd generation nets in comparison to the 2nd generation is reduced in near-scanning scene as collected by UAV.

In woodland environment, if the net concealed a target in realistic setting (i.e. conceal a vehicle in the wood),

the advantage of 3rd generation over 2nd generation camouflage net as countermeasure to hyperspectral imaging is not demonstrated.

In general, using the Glana L-4 it is possible to detect camouflaged target at low to medium noisy scene, if the target is purely presented in the pixel or at low mixing rate (i.e. 90% target and 10% background). At high mixing rate, it is difficult to detect camouflaged target in noisy scene. The detection performance of camouflage nets in operational scene is not only dependent on the spectral and spatial resolutions of the sensor. It is highly dependent on the detecting methods and the way they are implemented (i.e. in-scene spectra, library spectra, background pixels versus target pixels etcetera).

Although the observed limitation of large temporal gap between the bands, the capacity, affordability, simplicity, small size and accessibility of the Glana L-4 sensor makes it a good candidate for military operation in woodland environment.
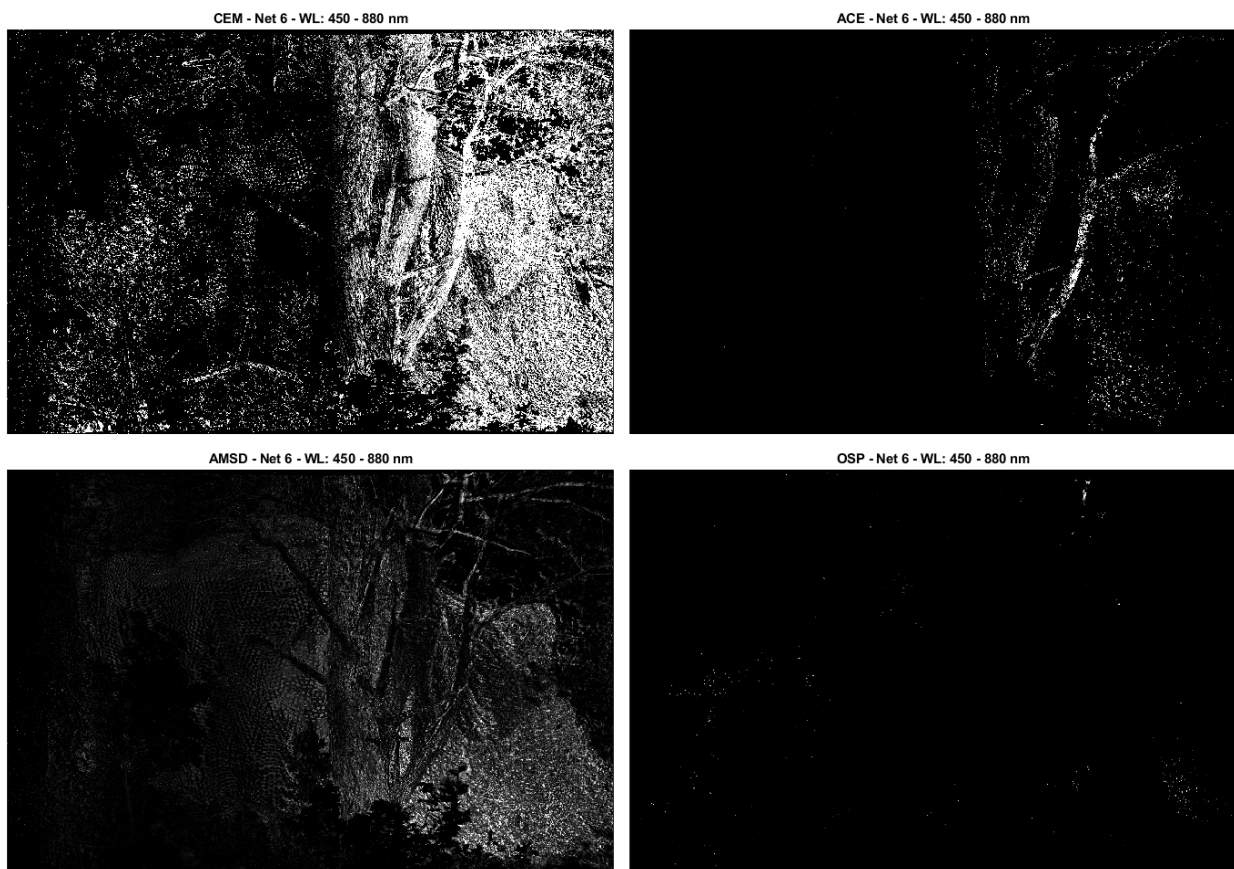
Figure 4-13: Scenario-3 - detection with known spectra of Net-6.

6.0   REFERENCES

[1]. W. Hua, T. Guo and X. Liu, "Camouflage target reconnaissance based on hyperspectral imaging technology," *In Proc. SPIE Optoelectronic Imaging and Processing Technology*, 9622, 2015.

[2]. Defense Industry, *Special report on next generation air and naval countermeasures*, p. 4, 2013.

[3]. M. Szustakowski, M. Ciurapinski, W. M. Zyczkowski, M. Palka, N. Kastek, M. Dulski, R. Bieszczad and G. Sosnowski, "Multispectral system for perimeter protection of stationary and moving objects," *In Proc. of SPIE* 7481, 74810D, 2009.

[4]. T. Müller, M. Müller and V. Cart, "Recent advancements in computer aided camouflage assessment," *In Proc. of SPIE* 8014, 2011.

[5]. D. H. Titterton and S. R. Carpenter, "The development of an imaging infrared surrogate seeker," *The Imaging Science Journal*, 58(5), pp. 269-275, 2013.

[6]. I. G. Renhorn, D. Bergstrom, J. Hedborg, D. Letalick and a. S. Moller, "High spatial resolution hyperspectral camera based on a linear variable Filter," *Optical Engineering*, 55(11), 2016.

[7]. I. G. Renhorn and Linnéa Axelsson "High spatial resolution hyperspectral camera based on exponentially variable filter," Optical Engineering 58(10), 103106 (29 October 2019). https://doi.org/10.1117/1.OE.58.10.103106

[8]. D. Manolakis, "Taxonomy of detection algorithms for hyperspectral imaging applications," *Optical Engineering*, 44 (6), 066403, 2005.

[9]. H. Huang, H. Qin, S. Yoo and D. Yu, "Local anomaly descriptor: A robust unsupervised algorithm for anomaly detection based on diffusion space", *In Proc. 21st ACM International Conference on Information and Knowledge Management, CIKM 2012; Maui, HI; United States*; 29 October 2012 - 2 November 2012, Pages 404-415.

[10]. D. Borghys, I. Kåsen, V. Achard, and C. Perneel, "Hyperspectral Anomaly Detection: Comparative Evaluation in Scenes with Diverse Complexity," *Journal of Electrical and Computer Engineering*, vol. 2012, Article ID 162106, 16 pages, 2012. https://doi.org/10.1155/2012/162106.

[11]. S. Shanmugam and P. Srinivasa Perumal, "Spectral matching approaches in hyperspectral image processing," *International Journal of Remote Sensing*, 35(24), 8217-8251, 2014 DOI:10.1080/01431161.2014.980922.

[12]. R.F. Kokaly, R.N. Clark, G.A. Swayze, K.E. Livo, T.M. Hoefen, N.C. Pearson, R.A. Wise, W.M. Benzel, H.A. Lowers, R.L. Driscoll, and A.J. Klein, *USGS Spectral Library Version 7: U.S. Geological Survey Data Series 1035*, 61 p., 2017, https://doi.org/10.3133/ds1035.

[13]. G. Wang, Y. Zhang, B. He and K. T. Chong, "A Framework of Target Detection in Hyperspectral Imagery Based on Blind Source Extraction," *IEEE Journal of Selected Topics in Applied Earth Observations and Remote Sensing*, 9 (2), pp. 835-844, 2016.

[14]. Nasser M. Nasrabadi, "Hyperspectral target detection," *IEEE Signal Processing Magazine* [34] January 2014.

[15]. Ronald G. Driggers, Van Hodgkin, Richard Vollmerhausen, "What good is SWIR? Passive day comparison of VIS, NIR, and SWIR," *Proc. SPIE 8706, Infrared Imaging Systems: Design, Analysis, Modeling, and Testing XXIV*, 87060L (10 June 2013); doi: 10.1117/12.2016467